QUASICRYSTALLINE BEAM FORMATION IN RF PHOTOINJECTORS*

J.B. Rosenzweig, M.P. Dunning, Erik Hemsing, G. Marcus, Pietro Musumeci, Agostino Marinelli,
UCLA Dept. of Physics and Astronomy, Los Angeles, CA 90034 USA,
M. Ferrario, INFN-LNF, Frascati (Roma) Italia

Abstract

The recent observation of coherent optical transition radiation at the LCLS has raised serious questions concerning the present model of beam dynamics in RF photoinjectors. We present here an analysis of what we term quasicrystalline beam formation. In this scenario, the low longitudinal temperature, in combination with strong acceleration and temporal rearrangement due to bending, allows the longitudinal beam dimension to become more regular, on the microscopic scale of optical wavelengths, than expected from equilibrium statistical properties. This beam distribution then may then display a strong degree of coherence in its optical transition radiation output. We discuss further experimental investigations of this phenomenon.

INTRODUCTION

The phenomenon of coherent optical transition radiation (COTR), observed at the LCLS [1] as well as numerous other labs worldwide, has attracted much attention recently. This previously unexpected effect has challenged the high brightness beam and FEL communities' understanding of the underlying physical mechanisms.

In order to clarify the scenario we are presented with, we recapitulate many of the observations from the LCLS photoinjector. First, OTR beam profile monitors upstream of the first bends behave as expected giving incoherent OTR that may be easily imaged to obtain accurate profiles. After the initial bends, a 45° two dipole system having transport matrix element $R_{56} \equiv \partial \zeta_f / \partial (\delta p / p)_i = 7$ mm that gives dispersion free conditions downstream, on the other hand many inter-related effects are seen that indicate coherence. These include: an integrated intensity dependence stronger than the number of electrons N; stochastic behavior in both the local intensity and the total radiated power; diffraction-style ring formation, and evidence for spectral spikes — enhancement of particular wavelengths.

The radiated energy enhancement after the initial bends produces up to four times enhancement in the OTR output even in the absence of added R_{56} due to the bunch compressors BC1 and BC2. This enhancement may be destroyed by detuning a dispersion matching quad in the first bends. With a larger R_{56} due to BC1 up to two orders of magnitude increase in OTR output is noted.

These dramatic effects have the practical effect of removing the utility of the OTR profile monitors, but also represent a fundamental challenge to the present models of collective dynamics in high brightness electron beams. As such, a number of hypotheses have been put forward to explain the observed signals. The most common of these states that there are either very short length structures in the beam distribution (spikes), or optical microbunching, in which the particles are clustered in a periodic manner. Further, these scenarios invoke longitudinal space-charge as an instigator of the micro-bunching, which along with bending effects such as coherent synchrotron radiation (CSR), produce a type of instability. This instability is both revealed and enhanced by the longitudinal rearranges induced by positive R_{56} associated with the bending systems.

Here, we propose a different point of view, that the beam is not classically microbunched, but rather has 1D crystalline characteristics, formed in novel manner, such that we term the state *quasi-crystalline beam* (QCB). In order to estimate the possible properties of a Coulomb crystal (intense beams are a relativistic example of such a system), we will have need first and foremost to make a simple calculation, that of the mean interparticle distance λ. If one begins with a macroscopic observable parameter, the beam density n_b, it is immediately apparent that one may write $\lambda = n_b^{-1/3}$. Considering a relevant example, that of the beam in the middle the end of the photoinjector post-acceleration linac (under invariant envelope conditions [2]) in the LCLS, one has $\lambda \cong 600$ nm, very close to the peaks observed in the COTR spectrum.

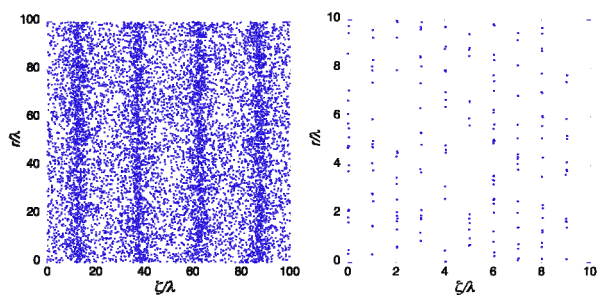

Figure 1. (left) Microbunched (in ζ) distribution example, with period of 25λ; (right) one-dimensional crystalline distribution, with natural periodicity of λ.

There are two critical points here derived from COTR observation: the spectrum is coherent in the optical, and there is compelling evidence for relatively narrow peaks, rather than broadband radiation. With peaks, one must have a periodic distribution, not simply very narrow (sub-fsec) isolated spikes. If the periodic distribution is much longer than λ, then there is a density wave associated with it, in which peaks in density are associated with closer relative spacing in the microbunched (in $\zeta = z - v_b t$)

* Department of Energy Basic Energy Science contract DOE DE-FG02-07ER46272, and Office of Naval Research contract ONR N00014-06-1-0925.

distribution, as shown in Fig. 1. However, a cold crystalline distribution (also given in Fig. 1, right) represents complete regularity in the spacing of the distribution. Its periodicity is given by the nearly uniform spacing of the particles in ζ. This picture is that of a 1D Coulomb crystal [3], which is organized in ζ and random in transverse coordinate *r*. One clearly needs descriptions of both the beam dynamics and observed radiation effects at the *microscopic* level, that of λ, as smooth distributions have no valid use in the cases of interest to us.

COULOMB CRYSTALS

A collection of charged particles, if it is hot and tenuous, behaves as a gas. When it becomes very dense and cool, as is the case in photoinjectors, the collective behavior is classified as that of a plasma (single component, with a relativistic drift, in the case of a beam), which has liquid characteristics. Finally, a Coulomb crystal is formed when one cools the collection of charged particles enough, so that the mean kinetic energy $k_B T$ is much smaller than the nearest-neighbor electrostical potential energy, $V = e^2/\lambda = e^2 n_0^{1/3}$. The crystal, which may take on a variety of simple forms (*e.g.* the bcc array shown in Fig. 2) is thus formed when the parameter (in beams defined in the rest frame) $\Gamma \equiv e^2 n_0^{1/3}/k_B T >> 1$.

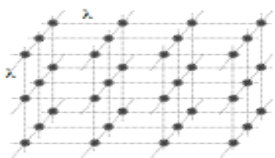

Figure 2. Schematic of 3D Coulomb crystal.

In beams, it is understood that 3D crystals such as that illustrated in Fig. 2 are easily formed. This is because in the transverse dimension the forces are applied in a time-dependent fashion, leading to crystal breakdown and heating. Nonetheless, 1D crystalline structures, such as that shown in Fig. 1, are more commonly encountered in beams. One of the hallmarks of such a 1D crystalline beam is that of the observed Schottky spectrum, which is a reflection of the distribution of interparticle spacing. When a beam is cooled to below the threshold temperature, the noise spectrum per se drops, while a strong coherent signal is observed at wavelengths of λ and its harmonics. We will return to this point below.

To begin examination of the LCLS case, we go to the rest frame of the beam and calculate Γ at the entrance of the photoinjector post-acceleration linac, using the following parameters: $k_B T$ =1 eV (cathode temperature), γ=11, $\sigma_x = 0.5$ mm, *I*=100 A, we obtain $\Gamma \cong 6\times10^{-4}$, which is far too small to yield even a 1D crystal. The condition Γ>>1 implies that particles do not cross each other's positions; in a true crystal this means that charged particles oscillate around their nominal lattice positions, with the characteristic frequency $\omega_p = \sqrt{4\pi e^2 n_0/m}$, the plasma frequency.

This nominal picture is changed dramatically by acceleration, however. Examining again the beginning of post-acceleration in the linac, and assuming a 14 MV/m accelerating field encountered suddenly (compared to a mean distance to overtaking) in structure, an electron leading a second electron by λ (in the nominal rest-frame) will gain 25 eV before the trailing electron begins its acceleration. The lead electron stretches its separation from the trailer, and continues to move away; this is of course the cause of relativistic electron beams having roughly invariant length in the lab frame, but enhanced by γ in the rest frame.

The summed effect is that thermal particles cannot overtake each other, due to this stretching phenomenon. In the lab, this is observed as a near freezing of the relative longitudinal positions of the electrons. This freezing, which we will quantify in the next section, is a critical component of what we term quasi-crystal formation. It serves to nearly lock in the non-uniformities in the beam's initial distribution, which give rise to repulsive space-charge forces. In a standard plasma, this effect leads through subsequent motion to the macroscopic density becoming more uniform. In the present case, there is little subsequent motion until a non-zero R_{56} is applied. If this R_{56} is optimized, strong microscopic ordering is obtained, analogous to the uniformity of a standard plasma after ¼ of a plasma period.

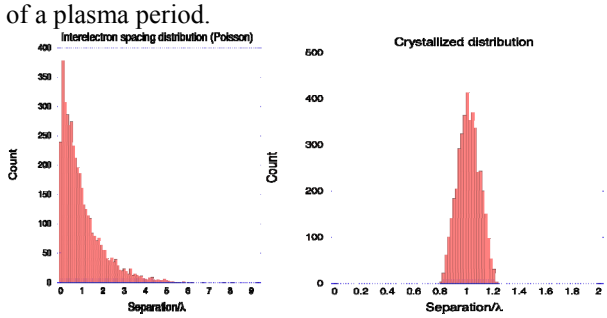

Figure 3. (left) Interparticle spacing distribution for random positions (Poisson); (right) crystal-type spacing distribution obtained by transform-ation described in text.

The dramatic change in the microscopic placement of particles that undergo this type of transformation can be quantified by examining the distribution of interparticle spacings, as given in Fig. 3. An initial random ordering of particles gives a Poisson distribution with most common separation being λ. On the other hand, after we apply the type of transformation described above in a nearly optimized way, the distribution of separations between neighbors becomes strongly clustered about λ. An example of this new type of distribution is also shown in Fig. 3. It is termed a quasicrystal, not a true crystal, because of its unique formation mechanism.

As mentioned above these distributions produce decidedly different radiation spectra. As the TR spectrum is expected to directly reflect the beam spectrum at the energies in question, we simply examine the beam spectra in the cases given in Fig. 3, shown in Fig. 4.

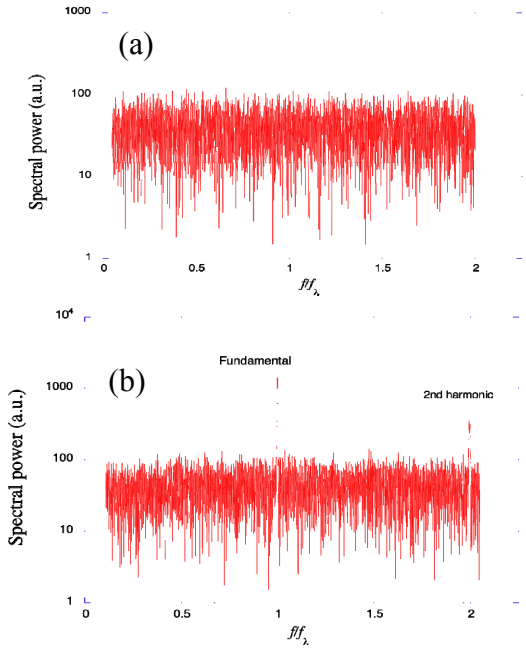

Figure 4. Beam power spectrum calculated for (a) random distribution and (b) quasicrystalline distributions of Fig. 3.

There is a significant enhancement of the power at λ and its harmonics. There is a concomitant lowering of noise level, which is notable in this 1D picture, but may be a bit subtle to measure in the actual experiments.

COLLECTIVE DYNAMICS

While there are obvious three-dimensional aspects to the beam we are examining (non-uniform densities, finite width effects, etc.), we reserve their discussion for later. Here, for illustrative purposes, we introduce a 1D model, assuming uniform fields given by very wide charge sheets of surface charge density σ (where $\sigma = -en_b\lambda$, in which case the fields are given by $\pm 2\pi\sigma$. We perform the analysis in the lab frame, in usual beam physics fashion. In this analysis, one follows the individual positions of the charge sheets, and assumes laminar flow — no overtaking, in which case the field depends only on the initial relative electron positions ζ.

In general, we then write that

$$\zeta'' + 3\frac{\gamma'}{\gamma}\zeta' + k_s^2\zeta = k_{p0}^2 F(\zeta_0), \text{ where } k_s^2 = \frac{k_{RF}\gamma'}{\gamma^3}\sin(\phi_0), \quad [1]$$

$k_{p0}^2 = \omega_p^2 / v_b^2 \cong \omega_p^2 / c^2$, $\gamma' = eE_{RF} / m_e c^2$, $k_{RF} = 2\pi / \lambda_{RF}$, and ϕ_0 is the phase of the beam with respect to RF crest. The 2nd term on the LHS of Eq. 1 corresponds to the strong damping of the ζ motion, while the 3rd term is due to RF focusing. The space-charge defocusing term on the RHS is given by the initial electron ordering, as

$$F(\zeta_0) = \frac{\sigma}{2n_b}\sum_i \left[\Theta(\zeta_0 - \zeta_i) - \Theta(\zeta_i - \zeta_0)\right]. \quad [2]$$

We can use this formalism to examine the motion of the charge sheets about an equilibrium (ideal crystal) position that requires the macroscopic component of space charge forces are cancelled by the RF focusing. Thus only microscopic motion remains. If one further assumes, as in the LCLS case, that the beam is run on the invariant envelope, with a size given by $a(\gamma) \cong \frac{4}{\gamma'}\sqrt{\frac{I}{3I_0\gamma}}$, we have

$$\Delta\zeta'' + 3\frac{\gamma'}{\gamma}\Delta\zeta' + \frac{3}{4}\left(\frac{\gamma'}{\gamma}\right)^2\Delta\zeta = 0, \quad [3]$$

is similar to transverse oscillations about the invariant envelope, but with stronger damping.

Solving this expression for the LCLS example, from the linac entrance to final energy before the first bend, we obtain the result in Fig. 5. We note that this 1D model over-estimates the space-charge force, and thus the motion of the charge sheets. Nevertheless, assuming an initial position error $\Delta\zeta_0$ at the linac entrance, the space-charge forces are not predicted to allow $\Delta\zeta$ to approach zero in the LCLS case. Thus the observation that there is negligible coherent enhancement of the observed OTR before the first bends is born out in this model.

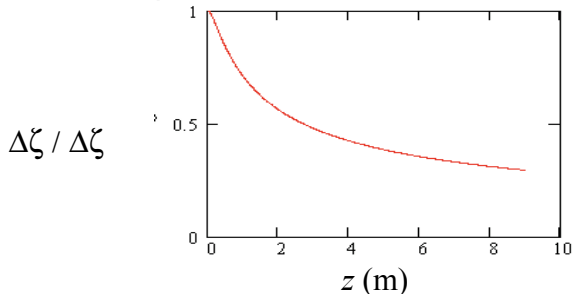

Figure 5. Solution for $\Delta\zeta$ in LCLS photo-injector case, beginning at linac entrance.

THREE-DIMENSIONAL EFFECTS

The 1D model discussed above has many defects, of course. The beam distribution is not transversely uniform and thus the "frozen field" is not uniform in x and y. This non-uniformity is mitigated by the mixing of particles due to transverse nonlaminarity, which while not significant macroscopically in a space-charge dominated beam, is expected at the level of λ.

The beam longitudinal forces are also made more uniform by the stretching of the distrib-ution in the beam Lorentz frame. This is because as the distribution stretches, particles within a transverse area $\sim(\gamma\lambda)^2$ contribute fields coherently to an electron separated from them in ζ by λ. Thus the maximum coherent field can be estimated to be independent of γ,

$$E_{z,sc} \approx \frac{r_e m_e c^2}{\lambda^2} \approx 120 \text{ V/m}, \quad [4]$$

with the example taken as the LCLS case. The increase in uniformity is enhanced further at higher energy due to the decrease in transverse beam size. As the acceleration field and space-charge fields are both roughly constant, the relative energy spread for a given separation of λ is also constant, $\|E_{z,sc}\| / E_{z,RF} \cong 10^{-5}$.

It is instructive to examine the implications this energy difference has on quasicrystal formation. In order to yield

ordering, one must apply the chicane transformation, to give a displacement $R_{56}\|E_{z,sc}\|/E_{z,RF}$, that moves the electron towards its optimum position. After the initial bends at LCLS, this displacement is estimated as 70 nm, which provides some notable motion towards quasi-crystal formation. After BC1, which has $R_{56} \sim 39$ mm, there is an estimated maximum displacement of 460 nm, quite near $\lambda/2$, as one expects from this model.

We have used at this point a very small beam temperature of 1 eV. In simulations, as well as initial (difficult) observations, one deduces much larger slice energy spreads of ~ 1 keV. However, these are not thermal spreads, rather they are correlated in *r,* due to differential acceleration from non-relativistic phase velocity spatial harmonics in the gun RF field. Thus there is a correlated shear force applied to any 1D crystalline structure created.

This assertion brings us to the point of describing likely crystallization structures in the actual, as opposed to 1D model, case. As the density is not uniform, and there are a number of effects which may cause different parts of the beam to create local structures, in both ζ and transverse coordinates. Thus one may expect that a number of local sub-structures, similar to grains in solids, to be formed in the beam that may have differing crystal periodicity. Evidence for this type of behavior has been observed at the LCLS [4] and at FLASH [5].

EXPERIMENTS AND SIMULATIONS

The core problem presented in trying to understand the validity of any microscopic model is, in the absence of ultrafine-resolution diagnostics, to correlate it to macroscopic measurements. It is interesting first to interpret the results of the initial LCLS observations, which have a factor of 4 in the ratio of coherent photons, estimated as

$$N_{CTR} \approx \frac{\alpha N^2 b^2}{4\sqrt{\pi} k_r \sigma_z}\left(\frac{\gamma}{k_r \sigma_x}\right)^4, \qquad [5]$$

where b is the bunching factor, to incoherent TR photons, $N_{TR} \approx \frac{\alpha N}{4\pi} BW$, where BW is the relative incoherent bandwidth. Here we have assumed that the "bunching", interpreted as the degree of crystallization is uniform across the beam, as in FEL case. The factor $\gamma/k_r\sigma_x$ ($k_r = 2\pi/\lambda$) is quite small, reflecting the fact that a uniformly bunched, transverse Gaussian-shaped many wavelengths across naturally radiates coherently only at small angles, $\theta_{\text{coh}} < 1/k_r\sigma_x$. This scenario is illustrated in Fig. 6, where the coherent part (which must be multiplied by the number of beam electrons N) occupies very little of the natural angular spread $\theta_{\text{TR}} < 1/\gamma$ of the TR.

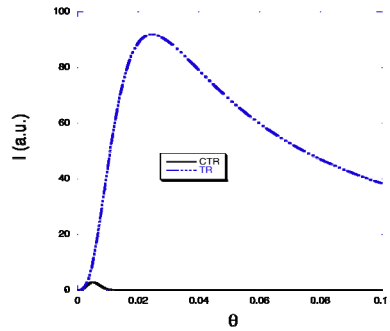

Figure 6. Incoherent and coherent (divided by N) components of CTR in LCLS case, no transverse variation of crystalline "bunching".

With Eq. 5, and the LCLS parameters, one deduces a value of b of 0.7%. However, with the grain picture discussed above, the efficiency of creating coherent light, which would show up as diffraction rings and speckle at angles up to γ^{-1}. Transverse structures smaller than the beam size will produce more off-axis coherent emission. In fact, the transverse COTR intensity pattern would be related to the transverse distribution as a Fourier transform, superimposed on the TR curve shape of Fig. 6. Thus a far-field angular distribution acts analogously to the frequency spectrum, which is a simple Fourier transform (because single-electron TR is flat in frequency) of the longitudinal distribution.

Thus, in future experiments, the coherent angular and wavelength spectra should reveal in detail the beam microscopic structures. In order to provide predictions for these spectra, we are developing a molecular dynamics code [3] that will allow simulation of the electron distribution at the single particle level. Results from this code will be presented in a subsequent work.

REFERENCES

[1] R. Akre, et al., Phys. Rev. ST Accel Beams, 11, 030703 (2008)
[2] Luca Serafini and James Rosenzweig Physical Review E 55, 7565 (1997).
[3] D. A. Krestnikov, et al., Proc. EPAC 2008, 1747 (JACOW, 2008)
[4] J. Frisch, *et al*., these proceedings.
[5] B. Schmidt, *et al*., these proceedings.